ResearchGate

See discussions, stats, and author profiles for this publication at: https://www.researchgate.net/publication/231648996

Dependence of Thermal Stability of Antiferromagnetic Nanocrystals on Size and Magnetic Proximity Effect

ARTICLE *in* THE JOURNAL OF PHYSICAL CHEMISTRY C · FEBRUARY 2008

Impact Factor: 4.77 · DOI: 10.1021/jp710759m

CITATIONS
3

READS
48

3 AUTHORS, INCLUDING:

Xing You Lang
Jilin University
46 PUBLICATIONS **1,662** CITATIONS
SEE PROFILE

Qing Jiang
Jilin University
502 PUBLICATIONS **8,526** CITATIONS
SEE PROFILE

Available from: Xing You Lang
Retrieved on: 01 February 2016

Dependence of Thermal Stability of Antiferromagnetic Nanocrystals on Size and Magnetic Proximity Effect

X. Y. Lang, Z. Wen, and Q. Jiang*

Key Laboratory of Automobile Materials (Jilin University), Ministry of Education, and Department of Materials Science and Engineering, Jilin University, Changchun 130022, China

Received: November 10, 2007; In Final Form: December 18, 2007

The thermal stabilities of antiferromagnetic (AFM) nanocrystals are dramatically different from those of their bulk counterparts. To understand the underlying mechanisms and factors that dominate the general trend of the tunability, the authors have established an analytic and simple model for the size and magnetic proximity effects on the thermal stability of AFM nanocrystals. This model has predicted size-induced undercooling and superheating in the Néel transition of AFM nanocrystals in bare nanoparticles, nanowires or nanorods, and thin films supported by nonmagnetic and magnetic substrates. The model enables us to reproduce the available experimental results of Ho, NiO, MnO, CuO, Co_3O_4, CoO, NiF_2, and FeF_2 AFM nanocrystals without any adjustable parameter.

Introduction

Antiferromagnetic (AFM) nanocrystals have recently gained increased attention by virtue of not only chemical stability[1] but also fundamental studies and potential device applications.[2] It is well known that the properties of AFM nanocrystals are dramatically different from those of their bulk counterparts because of the involvement of a high portion of spin coordination imperfection in the surface and interface. This opens fascinating possibilities for engineering of magnetic metamaterials with desired magnetic properties, which have led to a surge in both experimental and theoretical investigations.[3] It is important for understanding of the thermodynamic behavior of AFM nanocrystals because their thermal stability is of concern for the design of magnetic devices and governs the choice of the materials.

The thermal stability of AFM nanocrystals is indicated by the Néel temperature [$T_N(D)$] at which the thermal agitation energy is comparable to the exchange energy $E_{exc}(D)$ and eventually AFM ordering disappears, where D denotes the diameter of nanoparticles and nanorods, and the thickness of thin films. The reduced $T_N(D)$ function with D is a well-known phenomenon of AFM nanocrystals. For free-standing AFM nanocrystals, or AFM nanocrystals embedded in or supported by a nonmagnetic (NM) matrix, their $T_N(D)$ function decreases continuously with dropping D owing to the increase of surface (interface)/volume ratio, as observed in systems of FeF_2/ZnF_2 superlattices,[4,5] and CoO/SiO_2,[7,8] CoO/MgO,[9] NiO/MgO,[9,10] Ho/Nb/Y, and Ho/Y/Nb thin films,[11] as well as NiO,[12] CoO,[13] and MnO nanoparticles,[14] and CuO and Co_3O_4 nanoparticles[1,15−18] and nanorods.[1,19] Compared with AFM/NM superlattices,[4−6] AFM/AFM or AFM/ferromagnetic (FM) superlattices, for the examples of FeF_2/CoF_2,[20] NiO/CoO,[21] FeMn/Co,[22] FeMn/Ni, and FeMn/Ni/Co,[23] have revealed weaker finite-size effects because of the interlayer magnetic coupling.[24−27] Alternatively, for the thin AFM films deposited on bulk AFM or FM substrates,[9,19,28,29] the function of $T_N(D)$ of AFM films increases with dropping D because of the magnetic vicinity effect at AFM/FM interfaces, where the exchange coupling of AFM is enhanced.[9,19,28,29]

Two theoretical models have been proposed to illustrate the $T_N(D)$ functions of AFM nanocrystals. One is the finite-size scaling law,[30] which had been employed for thin CoO films[7]

$$T_N(D)/T_N(\infty) = 1 - (\xi_0/D)^{\lambda} \quad (1)$$

This equation is obtained from the temperature-dependent spin−spin correlation length function of $\xi(T) = \xi_0[1 - T/T_N(\infty)]^{-\nu}$ [7,30] where $\xi(T)$ denotes a distance from one point beyond which there is no further correlation of a physical property associated with the point. In eq 1, ∞ denotes the bulk size, T shows the absolute temperature, ξ_0 is the extrapolated correlation length at $T = 0$ K, and $\lambda = 1/\nu$ is the so-called shift exponent with ν being the critical exponent of the magnetic correlation length.

Another for $T_N(D)$ function is the empirical relation for Ho[11] and Cr thin films[31,32]

$$T_N(\infty)/T_N(D) = 1 + C_0'(D - D_0')^{-\lambda'} \quad (2)$$

where C_0' is a constant, D_0' represents the zero offset in the finite thickness of films, and λ' is a nonuniversal parameter.[11,31,32]

Although they provide reasonable descriptions of experimental results for size-induced undercooling in the Néel transition with the aid of adjustable free parameters, eqs 1 and 2 are strictly valid only for thicker homogeneous magnetic films.[3] In this process, the utilization of free parameters could mislead understandings of the related physical nature and the underlying mechanism and factors of $T_N(D)$ functions. Moreover, eqs 1 and 2 are invalid to explain the superheating phenomenon of $T_N(D)$ because of neglect of the magnetic proximity effect. Thus, deeper and consistent insight into the mechanism behind the unusual observations and finding factors are highly desirable because of the fundamentally great importance for advancing technological applications.

* Corresponding author. Fax: +86-431-85095876. E-mail: jiangq@jlu.edu.cn.

10.1021/jp710759m CCC: $40.75 © 2008 American Chemical Society
Published on Web 02/23/2008

In this contribution, a simple and unified model is established for size and magnetic proximity effects on the thermal stability of AFM nanocrystals. This unification certainly gives rise to the comprehension of thermal stability of magnetic nanocrystals. The model predictions are consistent with available experimental results.

Model

A simple AFM crystal can be visualized as consisting of two magnetic sublattices A and B such that the nearest neighbors of the atoms of A are atoms belonging to B, and vice versa.[33] Any atomic magnetic moments belonging to different sublattices have an antiparallel orientation with an AFM exchange constant or exchange coefficient ($J_{exc} < 0$). As temperature T increases, the thermal agitation energy begins to become comparable to E_{exc} and eventually AFM ordering disappears at T_N. On the basis of mean field approximation, there is[33]

$$k_B T_N(\infty) = -(2/3)\, J_{exc}(\infty)\, S(S+1) \tag{3}$$

where S is the spin of system and k_B is Boltzmann's constant.

In magnetic materials, the spins are coupled through the strong, short-range exchange interactions. $J_{exc}(\infty)$ between spins is strongly related to the overlap of the two atoms.[35] As indicated by the Bethe−Slater curve that had been confirmed by the quantum-mechanical calculations based on the Heitler−London approach,[36] the effective value of J_{exc} of AFM increases to zero as the distance between nearest neighbors increases to a certain value.[35] Alternatively, the atomic spacing increases when T is increased, which is related to the thermal agitation energy by the equipartition relation, namely, $m(2\pi\nu_E)^2\sigma^2(T) = k_B T$,[34] where m is the atomic mass, ν_E is the Einstein frequency, and $\sigma(T)$ is the root of mean-square displacement of atoms at T. Thus, at given T, each σ value should correspond to effectively temperature-dependent $J_{exc}(T,\infty)$. As $T \rightarrow T_N(\infty)$, $\sigma \rightarrow \sigma_N(\infty) = \{k_B T_N(\infty)/[m(2\pi\nu_E)^2]\}^{1/2}$ and $J_{exc}(T,\infty) \rightarrow J_{exc}(T_N,\infty)$, at which the Néel transition occurs. Note that $\sigma_N(\infty)$ denotes the bulk value of σ at $T_N(\infty)$. In light of the above consideration, the Néel transition of AFM crystals is assumed to occur when $\sigma_N(\infty)$ exceeds a fraction (p) of the atomic spacing (h). Namely, $\sigma_N(\infty)/h = p$, with $p \approx \{[T_N(\infty)/T_M(\infty)]^{1/2}\}/8$ on the basis of Lindemann's criterion for the melting of crystals, at which $\sigma_M(\infty) = \{k_B T_M(\infty)/[m(2\pi\nu_E)^2]\}^{1/2} \approx h/8$[34] with subscript M denoting the melting transition. This provides a convenient means for correlating $T_N(\infty)$ to measurable physical properties such as $\sigma^2(\infty)$, that is

$$\sigma^2(\infty) \propto T/T_N(\infty) \tag{4}$$

If this hypothesis is valid qualitatively for an AFM nanocrystal having the same crystalline structure as the bulk one, then the size-dependent $\sigma^2(D)$ function can be obtained by extending eq 4 to nanometer scale; that is, $\sigma^2(D) \propto T/T_N(D)$. Combining this relationship with eq 4 gives rise to

$$T_N(D)/T_N(\infty) = \sigma^2(\infty)/\sigma^2(D) \tag{5}$$

It is well known that the $\sigma^2(D)$ values of nanocrystals increase significantly in comparison with $\sigma^2(\infty)$[37−40] values as D is reduced, which results from the atomic coordination imperfection in the surface and the interface.[41] On the basis of the mean field approximation, the size-dependent function of the $\sigma^2(D)$ values of nanocrystals has been given by[42−44] $\sigma^2(D) = \sigma^2_v(D) + [\sigma^2_s(D) - \sigma^2_v(D)]n_s/n_t$, where subscript s and v denoting the surface atoms and the interior atoms of nanocrystals, and $n_s/n_t \propto 1/D$ is the ratio of the number of surface atoms (n_s) to the total atom number (n_t) of nanocrystals. If the cooperative coupling between the surface region and the interior region is phenomenologically considered by taking the variation of $\sigma^2(D)$ to be dependent on the value of $\sigma^2(D)$ itself, then a change in σ^2 can give rise to $\sigma^2(x + dx) - \sigma^2(x) = (\alpha_s - 1)\,\sigma^2(x)dx$, which is achieved by assuming that σ^2_s/σ^2_v are size-independent and $\alpha_s = \sigma^2_s(D)/\sigma^2_v(D) \approx \sigma^2_s(\infty)/\sigma^2_v(\infty)$, $x = n_s/n_v = D_0/(D - D_0)$ with D_0 denoting a critical size at which all of the atoms or molecules of low-dimensional nanocrystals are located on their surfaces.[42] In terms of the definition of D_0 and the bulk boundary condition, two asymptotic limits should be satisfied, namely $\sigma^2(D)/\sigma^2(\infty) \rightarrow 0$, when $D \rightarrow D_0$, and $\sigma^2(D)/\sigma^2(\infty) \rightarrow 1$, when $D \rightarrow \infty$. Associated with the conditions and integrating the above equation, it reads $\sigma^2(D)/\sigma^2(\infty) = \exp[(\alpha_s - 1)/(D/D_0 - 1)]$.[42−44] Substituting this equation into eq 5 induces

$$T_N(D)/T_N(\infty) = \exp[-(\alpha_s - 1)/(D/D_0 - 1)] \tag{6}$$

where D_0 is a function of dimension number d and normalized surface (interface) area c,[45] namely

$$D_0 = 2c(3 - d)h \tag{7}$$

For the free surface of nanocrystals, the parameter α has been determined by[45]

$$\alpha_s = 1 + [2S_{vib}(\infty)/(3R)] \tag{8}$$

As a rule, the overall melting entropy $S_m(\infty)$ consists, at least, of three contributions: positional $S_{pos}(\infty)$, vibrational $S_{vib}(\infty)$, and electric component $S_{el}(\infty)$[46]

$$S_m(\infty) = S_{vib}(\infty) + S_{pos}(\infty) + S_{el}(\infty) \tag{9}$$

The idea of $S_{pos}(\infty)$ of melting arises in connection with the positional disorder as a substance undergoes a transition from the solid state to the liquid state. The number of particle species naturally plays a primary role in the disordering process. In the case of simple solids, only two particle species are present: the atoms of the given substance and vacancies.[46] In this case, $S_{pos}(\infty)$ is given by[46]

$$S_{pos}(\infty) = -R(x_A \ln x_A + x_v \ln x_v) \tag{10}$$

where $x_A = 1/(1 + \Delta V_m/V_m)$ and $x_v = 1 - x_A$ are the molar fractions of the host material and vacancies, respectively, and ΔV_m is the molar volume difference between the liquid and the crystal.

For metallic crystals, the type of chemical connection does not change during the melting transition. Thus, $S_{el}(\infty) \approx 0$[46] and $S_{vib}(\infty) = S_m(\infty) - S_{pos}(\infty)$, or

$$S_{vib}(\infty) = S_m(\infty) + R(x_A \ln x_A + x_v \ln x_v) \tag{11}$$

For semi-metals, $S_{el}(\infty) \neq 0$, and $S_{vib}(\infty)$ must be determined in a direct way, that is, Mott's equation[47]

$$S_{vib}(\infty) = 3R \ln(\upsilon_s/\upsilon_l) = (3/2)R \ln(\mu_s/\mu_l) \tag{12}$$

where υ and μ denote the characteristic vibration frequency and the electrical conductivity, respectively. If the parameters in eq 12 are unavailable, then the following equation can also be employed as a first-order approximation:[46]

$$S_{vib}(\infty) = S_m(\infty) - R \tag{13}$$

For semiconductors, the melting is accompanied by the semiconductor-to-metallic transition and the elements or compounds suffer contraction in volume rather than expansion for most metals. Thus, $S_{el}(\infty)$ strongly contributes to $S_m(\infty)$, and $S_{pos}(\infty) \ll S_{el}(\infty)$. $S_{pos}(\infty)$ is thus negligible as a first-order approximation.[48] Namely

$$S_{vib}(\infty) = S_m(\infty) - S_{el}(\infty) \quad (14)$$

Note that eq 14 is invalid for some metallic mixing oxides, for instance, Fe_3O_4 consisting of $Fe_2O_3 + FeO$, which undergoes semiconductor-to-metal transition due to the Fe^{2+} and Fe^{3+} ions order on the *B* sites at 122 K (the so-called Verwey transition), while the melting temperature is far above the Verwey temperature.[49]

For systems consisting of AFM films and substrates, the magnetic proximity effect takes place at the interface between AFM films and substrates.[4−11,20−29,50] When two substances are in atomic contact with each other, it is quite natural to expect that a novel magnetic arrangement in this vicinity of the interface is different from the bulk one.[50] The parameter α_i of this interface must be considered, where subscript i denotes the interface. In terms of the definition of α, $\alpha_i = \sigma_i^2(D)/\sigma_v^2(D) = \alpha_s\sigma_i^2(D)/\sigma_s^2(D)$ with $\alpha_s = \sigma_s^2(D)/\sigma_v^2(D)$. On the basis of the assumption that $\sigma^2(D) \propto 1/J$,[45] $\sigma_s^2(D) \propto 1/J_s$, and $\sigma_i^2(D) \propto 1/J_i$, where J_s and J_i are the exchange coupling constants between spins located at surface of AFM films and between the spins of AFM and substrates, respectively. The former $J_s \propto T_N(\infty)$ and the latter $J_i \propto T_{sub/AFM}$, where $T_{sub/AFM}$ is the temperature corresponding to the exchange coupling constant between spins of AFM and substrates. $T_{sub/AFM}$ can be given proximately by $T_{sub/AFM} \propto [J_s^2 + J_{sub}^2 - 2J_sJ_{sub}\cos(180 - \theta)]^{1/2} \propto [T_N(\infty)^2 + T_{sub}(\infty)^2 - 2T_N(\infty)\, T_{sub}(\infty)\cos(180 - \theta)]^{1/2}$ with J_{sub} and T_{sub} denoting the exchange coupling constant of substrate substances and its corresponding temperature and θ representing the angle between FM and AFM spins. Note that the substrates can be magnetic ($T_{sub} \neq 0$ or $J_{sub} \neq 0$) materials and NM ($T_{sub} = 0$ or $J_{sub} = 0$) like noble metals, NM transition metals, semiconductors, as well as insulators. As a result, $\sigma_i^2(D)/\sigma_s^2(D) = J_s/J_i$, or

$$\alpha_i = \alpha_s T_N(\infty)/[T_N(\infty)^2 + T_{sub}{}^2 - 2T_N(\infty)T_{sub}\cos(180 - \theta)]^{1/2} \quad (15)$$

Considering both surface and interface effects on $T_N(D)$, eq 6 can be rewritten as

$$T_N(D)/T_N(\infty) = c\exp[-(\alpha_s - 1)/(D/D_0 - 1)] + (1 - c)\exp[-(\alpha_i - 1)/(D/D_0 - 1)] \quad (16)$$

Obviously, eq 16 can be used for bare and embedded nanocrystals with $c = 1$ and epitaxial AFM films on nonmagnetic or magnetic substrates with $c = 1/2$. For the latter, it should be mentioned that the side surface is neglected because the side surfaces have a small percentage of the total surface in comparison with that of the up surface and bottom interface of thin films.

Results and Discussion

Figure 1 presents $T_N(D)$ functions for MnO,[14] CuO,[1,15−17] NiO,[9,10] $NiCoO_2$,[9] and Ho nanocrystals[11] with comparisons between model prediction in terms of eq 16 and available experimental data, where the used parameters in the calculations are listed in Table 1. As shown in this figure, for free-standing nanoparticles, nanorods, and thin films deposited on NM substrates, a general trend of $T_N(D)$ functions is that T_N as a function of D reveals a continuous decrease.[1,3,11,14−17] Furthermore, the change of the $T_N(D)$ function of nanorods with D is weaker than that of nanoparticles but stronger than that of thin films. This results from different surface (interface)/volume ratio $A/V = 6/D$, $4/D$, $2/D$ for nanoparticles, nanorods, and thin films with $d = 0$, 1, 2, respectively.[45]

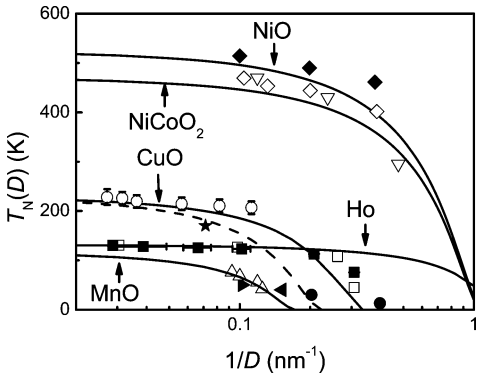

Figure 1. Comparisons of $T_N(D)$ functions between model predictions in terms of eq 16 and experimental data of NiO thin films (◆,[9] ◇,[9] ▽[10]), Ho thin films (■,[11] □[11]), CuO nanorods (●[1]) and nanoparticles (right-facing triangle[1] ○,[15] left-facing triangle,[16] ★[17]), and MnO nanoparticles (△[14]). The parameters: for NiO and Ho thin films, $D_0 =$ 0.8420 and 0.7154 nm in terms of eq 7 with $d = 2$ and $c = 1/2$, $\alpha_i = \alpha_s = 1.583$, 1.561 in light of eqs 8 and 15 with $T_{sub} = 0$, respectively; for CuO nanorods, CuO and MnO nanoparticles, $D_0 = 2.738$, 4.107, 5.328 nm with $d = 1$, 0 and $c = 1$, $\alpha_s = 1.563$, 1.502. The other parameters used in all figures are listed in Table 1.

TABLE 1: Parameters Utilized in the Calculations of Equation 16 about AFM Materials ($T_N(\infty)$ is in K, $S_{vib}(\infty)$ in J·g-atom^{-1}·K^{-1}, and h is in nm)[45]

	$T_N(\infty)$	$S_{vib}(\infty)$ [a]	h
CoO	315 [7]/293 [8,9]	6.789	0.852 [9]
Co_3O_4	40 [19]	6.452	0.807 [19]
CuO	229 [1]	7.016	0.684 [1]
FeF_2	79 [2,6]	5.724	0.664 [6]
NiF_2	80 [28]	6.554	0.938 [28]
Ho	131 [11]	6.999	0.715 [62]
MnO	117 [14]	6.261	0.888 [14]
NiO	523 [9,10]	7.271	0.842 [9]
FeMn	490 [2] /500 [22]	7.786	0.716 [22]

[a] $S_{vib}(\infty)$ of compounds and alloys of A_mB_n are given as $S_{vib,A_mB_n}(\infty) = [mS_{vib,A}(\infty) + nS_{vib,B}(\infty)]/(m + n)$ as a first approximation because no experimental data are found, where *A* and *B* denote compound or alloy atoms and *m* and *n* are the corresponding components, respectively.

Similar results can be observed in Figures 2−4 for FeF_2/ZnF_2 films,[6] Co_3O_4 nanoparticles[18] and nanorods,[19] and CoO thin films supported by SiO_2,[7,8] and MgO substrates,[9] respectively. It is well known that the depressed $T_N(D)$ of AFM nanocrystals is induced by a reduction in the number of spin interactions at the surface in comparison with that in the interior.[41,45,51,52] Therefore, the wide distribution of experimental results of $T_N(D)$[1,6−11,14−17,28,29] results from the different broken translational symmetries with different facets and coordination numbers, which induces the changes of $T_N(D)$ with different extent according to the classic broken-bond rule.[54] As shown in these figures, the model predictions are consistent with available experimental data.

For thin AFM films epitaxially grown on NM substrates with a small lattice misfit, where spin exchange interaction at the interface between AFM and NM substrate is assumed to be absent,[11] the depression of $T_N(D)$ should be attributed to the combined effect of both free surface and interface of films. The

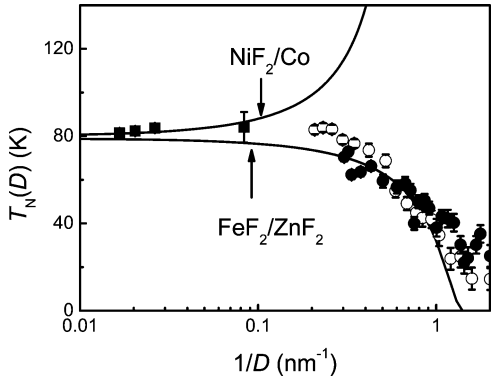

Figure 2. Comparisons of $T_N(D)$ functions of FeF_2 and NiF_2 between model predictions according to eq 16 and experimental measurements of FeF_2/ZnF_2 films (○,[6] ●[6]) and $MgF_2/NiF_2/Co$ films (■[28]). The parameters employed in the calculations of eq 16 are listed as D_0 = 0.664, 0.938 nm, and α_s = 1.459, 1.526 in terms of eq 7 with d = 2 and c = 1/2 and eq 8 for FeF_2, NiF_2, respectively. α_i = 0.0832 according to eq 15 with $T_{sub} = T_c$ = 1388 K for Co.[28]

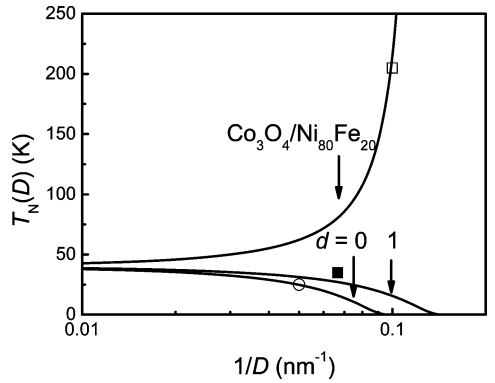

Figure 3. Comparisons of $T_N(D)$ functions of Co_3O_4 between model predictions in light of eq 16 and experimental evidence for Co_3O_4 nanoparticles (○[18]), nanorods (■[19]), and $Co_3O_4/Ni_{80}Fe_{20}$ films (□[19]), where the parameters D_0 = 4.842, 0.807 nm in terms of eq 7 with d = 0, 2 and c = 1, 1/2, respectively, α_i = 0.0722 according to eq 15 with α_s = 1.517, T_{sub} = 800 K for $Ni_{80}Fe_{20}$[19] and θ = 0°.[2]

AFM/NM interface has two effects on $T_N(D)$ functions: One is $\alpha_i = \alpha_s$ in terms of eq 15 with T_{sub} = 0 because the substrates are nonmagnetic,[3,11,45] which implies that the AFM/NM interface is similar to the free surface of AFM films, where the spin coordination number is lower than that in the interior.[11] The other is c = 1/2 in eq 7 because of the disappearance of one of the free surfaces of the films,[51] which results in a weaker decrease of the $T_N(D)$ values of epitaxial thin films compared with those of free-standing thin films with two free surfaces.[45,53]

However, for AFM/FM or AFM/AFM heterogeneous structures, the $T_N(D)$ functions of AFM films demonstrate dramatical variations with dropping D due to different magnetic proximity effects induced by magnetic substrates or covering layers. When AFM films are epitaxially deposited on FM or AFM bulk substrates with higher Curie or Néel temperature, a reverse trend of $T_N(D)$ functions is revealed; that is, the $T_N(D)$ of AFM films increases in comparison with $T_N(\infty)$ as D is reduced. This can be predicted in terms of eq 16 through taking the magnetic proximity effect into account, where $\alpha_i < 1 < \alpha_s$ in terms of eq 15 with $T_{sub} > T_N(\infty)$. It should be noted that the θ = 0 is assumed because of the strong magnetic proximity effect.[2] The comparisons between the model predictions and experimental evidence for $Co/CoF_2/MgF_2$,[28] $Co_3O_4/Ni_{80}Fe_{20}$,[19] and CoO/NiO[9] CoO/Fe_3O_4[29] are shown in Figures 2−4, respectively. It is evident that because of magnetic proximity effect at AFM/FM interfaces,[9,19,28,29] although the free surface of such CoF_2, Co_3O_4,

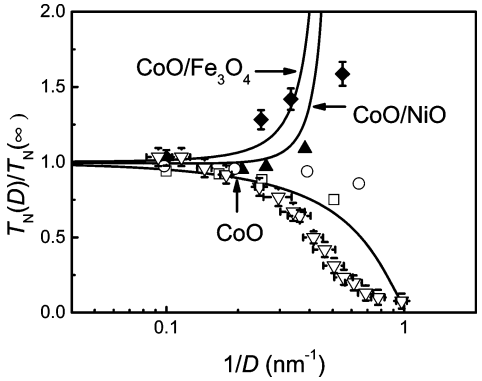

Figure 4. Comparisons of $T_N(D)$ functions of thin CoO films between eq 16 and experimental data for CoO/SiO_2 (▽[7,8]), CoO/MgO (□, ○[9]), CoO/NiO (▲[9]), CoO/Fe_3O_4 (◆[29]), where D_0 = 0.852 nm in terms of eq 7 with d = 2 and c = 1/2, α_i = 1.544, 0.4139, 0.5544 for CoO/NM, CoO/NiO, and CoO/Fe_3O_4 according to eq 15 with T_{sub} = 0, 523, 860 K for NM materials, NiO,[9] and Fe_3O_4,[45] respectively, and θ = 0°.[2]

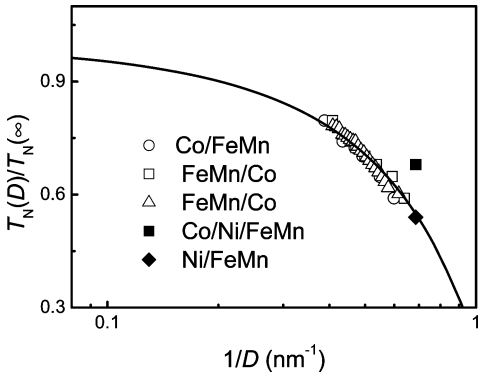

Figure 5. Comparisons of $T_N(D)$ functions of $Fe_{50}Mn_{50}$ between eq 16 and experimental data of $Fe_{50}Mn_{50}/Co/Cu(001)$,[22] $Ni/Fe_{50}Mn_{50}/Cu(001)$,[23] and $Co/Ni/Fe_{50}Mn_{50}/Cu(001)$,[23] where the parameters are listed as D_0 = 0.716 nm and α_s = 1.624 in terms of eq 8.

and CoO films still has a tendency to lower the $T_N(D)$ value of the films, the total effect of the free surface and the interface leads to the drop of the total energy of the film, and thus the increase of the $T_N(D)$ function with decreasing D. Furthermore, the stronger the interaction is at the interface, the more the $T_N(D)$ function increases.[9,29] This differs from the experimental results of Fe/Cr(001),[31,32] whose $T_N(D)$ decreases with dropping D, which could result from the spin-frustration effect in the vicinity of the rough Fe/Cr(001) interfaces where the interfacial exchange energy can be minimized only locally and frustration of the interfacial spins occurs because Fe and Cr have magnetical long-range order.[31,32]

Although for $Fe_{50}Mn_{50}$ films covered by ultrathin FM layers, such as Co (0.72 nm),[22] Ni (2.7 nm),[23] and Co(0.9 nm)/Ni(2.7 mL),[28] the magnetic proximity effect induced by the magnetic layer becomes too weak to induce the enhancement of $T_N(D)$ functions because the J_i or T_{sub} is small enough.[22,23,50] Because the films of $Fe_{50}Mn_{50}$ covered by FM or AFM layers exhibit single transition temperatures,[20] it is reasonable to consider them as AFM/AFM or AFM/FM superlattices. Therefore, weaker size-dependence of undercooling of $T_N(D)$ in comparison with that of AFM/NM heterogeneous structures can be observed. As shown in Figure 5, the model prediction is qualitatively consistent with the experimental data for the systems of $Fe_{50}Mn_{50}/Co/Cu(001)$,[22] $Ni/Fe_{50}Mn_{50}/Cu(001)$,[23] and $Co/Ni/Fe_{50}Mn_{50}/Cu(001)$.[23]

In terms of this model, the magnetic properties of AFM nanocrystals are strongly dependent on both CN and σ.[55] On

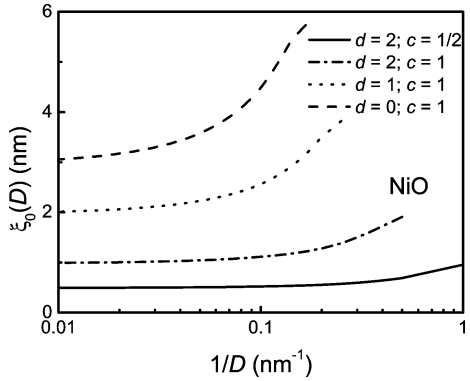

Figure 6. $\xi_0(D)$ functions in terms of eq 17 for NiO free-standing nanoparticles, nanorods, thin films, and films supported by substrates, respectively. The related parameters are the same as those listed in Figure 1 and Table 1.

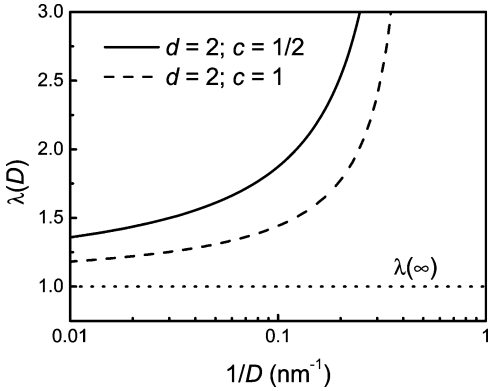

Figure 7. Shift exponent function $\lambda(D)$ in terms of eq 19 for free-standing and supported CoO films with $\xi_0 = 2.0$ nm.[7] The utilized parameters are the same as those listed in Figure 4 and Table 1.

one hand, as $T \rightarrow 0$ K and $\sigma \rightarrow 0$, the thermal effect is negligible, and the CN imperfection takes the premier role in determining the magnetic properties of nanocrystals. The latter gives rise to the contraction of atomic spacing in the light of the Pauling[56] and Goldschmidt premises.[57] This causes the spin electrons to be more localized, and produces larger magnetic moment per atom than bulk.[55,58] On the other hand, when $T \rightarrow T_N$, σ increasing to σ_N induces the absolute value of J_{exc} decreasing to zero[35] and the occurrence of the Néel transition. Because of the atomic CN reduction of freestanding nanocrystals, $\sigma(D)$ increases with dropping D at this temperature range.[37−40,59] Thus, the thermal energy needed to promote σ to increase to σ_N decreases, so does the $T_N(D)$ function.[1,6−11,14−17] For embedded AFM nanoparticles in magnetic matrix or AFM films epitaxially grown on magnetic substrates, the thermal stability of AFM nanocrystals increases with dropping D because of the strong depression induced by the strong magnetic proximity effect at the AFM/surrounding interface.[9,19,28,29] Thus, the thermal stability of AFM nanocrystals could increase or decrease depending on the AFM/surrounding interface situation. It is worth noting that for the sake of simplicity the existence of easy and hard axes and magnetocrystalline anisotropy are neglected in this model.

On the basis of the mean-field approximation, eq 1 can be rewritten as $T_N(D)/T_N(\infty) = 1 - \xi_0/D$ with $\lambda = 1$.[30] Combining this relationship and eq 16, one can obtain the size-dependent $\xi_0(D)$ function

$$\xi_0(D) = D\{1 - c\exp[-(\alpha_s - 1)/(D/D_0 - 1)] - (1 - c)\exp[-(\alpha_i - 1)/(D/D_0 - 1)]\} \quad (17)$$

Obviously, $\xi_0(D)$ is determined by both the naturally thermodynamic properties of AFM crystals $S_{vib}(\infty)$ and the interface condition in the heterogeneous structures. In terms of eq 17, the functions of $\xi_0(D)$ of NiO nanocrystals for free-standing nanoparticles, nanorods, thin films, and films supported by substrates, respectively, are shown in Figure 6. As observed in this figure, $\xi_0(D)$ decreases with increasing of D and then reaches a plateau. Because D is small enough, $\xi_0(D)$ depends not only on parameters c and d but also on the size of nanocrystals, whereas ξ_0 is a size-independent constant for $D \gg D_0$, namely, $\xi_0 = -c(\alpha_s - 1)D_0 + (1 - c)(\alpha_i - 1)D_0$. If we interpret the length scale $\xi_0(D)$ to characterize a near-surface layer,[41,60,61] then eq 17 indicates that the surface layer plays a more and more important role in the influence of the surface layer on the magnetic properties of AFM nanocrystals as D is reduced.

Considering the mathematical relationship of $\exp(-x) \approx 1 - x$ when x is small enough as a first-order approximation, eq 16 can be simplified as

$$T_N(D)/T_N(\infty) = 1 - [c(\alpha_s - 1) + (1 - c)(\alpha_i - 1)]D_0/D \quad (18)$$

Equation 18 indicates that the most important size effect on $T_N(D)$ relates closely to the surface/volume ratio of the AFM nanocrystals, or $1/D$ when $D > 10D_0$.

The value of λ in eq 1 under the non-mean-field approximation can be determined by comparing eq 1 with eq 18. Namely, $\lambda(D) = \{\ln D_0[c(\alpha_s - 1) + (1 - c)(\alpha_i - 1)] - \ln D\}/(\ln \xi_0 - \ln D)$, where ξ_0 is a constant in light of the above analysis.[7,52] As $D \rightarrow \infty$, $\lambda(\infty) \approx 1$. As a consequence

$$\lambda(D)/\lambda(\infty) = \{\ln D_0[c(\alpha_s - 1) + (1 - c)(\alpha_i - 1)] - \ln D\}/(\ln \xi_0 - \ln D) \quad (19)$$

In terms of eq 19, Figure 7 presents the model predictions of $\lambda(D)$ for thin CoO films with $\xi_0 = 2.0$ nm,[7] where the solid and dashed lines correspond to the freestanding and supported CoO thin films, respectively. Obviously, the $\lambda(D)$ function generally increases with decreasing D and c for the finite-size scaling law. If $\xi_0 = -c(\alpha_s - 1)D_0 + (1 - c)(\alpha_i - 1)D_0$ and $\lambda = 1$ in eq 1 based on the mean-field approximation, then eq 1 is the same as eq 18, in which the parameters are definitely physical, describing all $T_N(D)$ functions in AFM nanocrystals although eqs 1 and 18 are only valid for thicker AFM films with $D > 10D_0 \approx 7-9$ nm supported by substrates.[3]

Compared with the previous models,[7,11,31,32] this model without any adjustable parameter can be used to predict the effects of dimension and interface on the $T_N(D)$ function through introducing the parameters D_0 and α, respectively. As shown in these figures, complicated $T_N(D)$ values are still analyzed and predicted by this simple and unified model as long as the surface and interface conditions of the low-dimensional crystals and relative thermodynamic parameters are known.

Conclusions

In summary, a simple and unified theoretical model, without any adjustable parameter, has been established to describe the dependencies of the thermal stability of AFM nanocrystals on size and the magnetic proximity effect. In terms of this model, $T_N(D)$ functions decrease or increase with dropping D and d, depending on the interfacial conditions. This model interprets reasonably the size-induced undercooling and superheating in the Néel transition of AFM nanocrystals. The validity is

confirmed by the quantitative consistence between model predictions and available experimental data of Ho, NiO, MnO, CuO, Co_3O_4, CoO, NiF_2, and FeF_2 nanocrystals.

Acknowledgment. Financial support by National Key Basic Research and Development Program (Grant No. 2004CB619301), and by the "985 Project" of Jilin University are acknowledged.

References and Notes

(1) Zheng, X. G.; Xu, C. N.; Nishikubo, K.; Nishiyama, K.; Higemoto, W.; Moon, W. J.; Tanaka, E.; Otabe, E. S. *Phys. Rev. B* **2005**, *72*, 014464.
(2) Nogués, J.; Schuller, I. K. *J. Magn. Magn. Mater.* **1999**, *192*, 203.
(3) Jensen, P. J.; Bennemann, K. H. *Surf. Sci. Rep.* **2006**, *61*, 129.
(4) Lederman, D.; Ramos, C. A.; Jaccarino, V.; Cardy, J. L. *Phys. Rev. B* **1993**, *48*, 8365.
(5) Lederman, D.; Ramos, C. A.; Jaccarino, V. *J. Phys.: Condens. Matter* **1993**, *5*, A373.
(6) Yamazaki, H.; Satooka, J. *J. Magn. Magn. Mater.* **2002**, *240*, 442.
(7) Ambrose, T.; Chien, C. L. *Phys. Rev. Lett.* **1996**, *76*, 1743.
(8) Tang, Y. J.; Smith, D. J.; Zink, B. L.; Hellman, F.; Berkowitz, A. E. *Phys. Rev. B* **2003**, *67*, 054408.
(9) Abarra, E. N.; Takano, K.; Hellman, F.; Berkowitz, A. E. *Phys. Rev. Lett.* **1996**, *77*, 3451.
(10) Alders, D.; Tjeng, L. H.; Voogt, F. C.; Hibma, T.; Sawatzky, G. A.; Chen, C. T.; Vogel, J.; Sacchi, M.; Iacobucci, S. *Phys. Rev. B* **1998**, *57*, 11623.
(11) Weschke, E.; Ott, H.; Schierle, E.; Schüssler-Langeheine, C.; Vyalikh, D. V.; Kaindl, G.; Leiner, V.; Ay, M.; Schmitte, T.; Zabel, H.; Jensen, P. J. *Phys. Rev. Lett.* **2004**, *93*, 157204.
(12) Makhlouf, S. A.; Parker, F. T.; Spada, F. E.; Berkowitz, A. E. *J. Appl. Phys.* **1997**, *81*, 5561.
(13) Sako, S.; Ohshima, K.; Sakai, M.; Bandow, S. *Surf. Rev. Lett.* **1996**, *3*, 109.
(14) Sako, S.; Ohshima, K. *J. Phys. Soc. Jpn.* **1995**, *64*, 944.
(15) Punnoose, A.; Magnone, H.; Seehra, M. S.; Bonevich, J. *Phys. Rev. B* **2001**, *64*, 174420.
(16) Punnoose, A.; Seehra, M. S. *J. Appl. Phys.* **2002**, *91*, 7766.
(17) Stewart, S. J.; Multigner, M.; Marco, J. F.; Berry, F. J.; Hemando, A.; Gonzalez, J. M. *Solid State Commun.* **2004**, *130*, 247.
(18) Makhlouf, S. A. *J. Magn. Magn. Mater.* **2002**, *246*, 184.
(19) van Lierop, J.; Lin, K. W.; Guo, J. Y.; Ouyang, H.; Southern, B. W. *Phys. Rev. B* **2007**, *75*, 134409.
(20) Ramos, C. A.; Lederman, D.; King, A. R.; Jaccarino, V. *Phys. Rev. Lett.* **1990**, *65*, 2913.
(21) Takano, M.; Terashima, T.; Bando, Y.; Ikeda, H. *Appl. Phys. Lett.* **1987**, *51*, 205.
(22) Won, C.; Wu, Y. Z.; Zhao, H. W.; Scholl, A.; Doran, A.; Kim, W.; Owens, T. L.; Jin, X. F.; Qiu, Z. Q. *Phys. Rev. B* **2005**, *71*, 024406.
(23) Lenz, K.; Zander, S.; Kuch, W. *Phys. Rev. Lett.* **2007**, *98*, 237201.
(24) Carey, M. J.; Berkowitz, A. E.; Borchers, J. A.; Erwin, R. W. *Phys. Rev. B* **1993**, *47*, 9952.
(25) Borchers, J. A.; Carery, M. J.; Erwin, R. W.; Majkrzak, C. F.; Berkowitz, A. E. *Phys. Rev. Lett.* **1993**, *70*, 1878.
(26) Carriço, A. S.; Camley, R. E. *Phys. Rev. B* **1992**, *45*, 13117.
(27) Zhang, S. F.; Zhang, G. H. *J. Appl. Phys.* **1994**, *75*, 6685.
(28) Shi, H. T.; Lederman, D.; O'Donovan, K. V.; Borchers, J. A. *Phys. Rev. B* **2004**, *69*, 214416.
(29) van der Zaag, P. J.; Ijiri, Y.; Borchers, J. A.; Feiner, L. F.; Wolf, R. M.; Gaines, J. M.; Erwin, R. W.; Verheijen, M. A. *Phys. Rev. Lett.* **2000**, *84*, 6102.
(30) Fisher, M. E.; Barber, M. N. *Phys. Rev. Lett.* **1972**, *28*, 1516.
(31) Fullerton, E. E.; Riggs, K. T.; Sowers, C. H.; Bader, S. D. *Phys. Rev. Lett.* **1995**, *75*, 330.
(32) Fullerton, E. E.; Adenwalla, S.; Felcher, G. P.; Riggs, K. T.; Sowers, C. H.; Bader, S. D.; Robertson, J. L. *Physica B* **1996**, *221*, 370.
(33) Van Vleck, J. H. *Rev. Mod. Phys.* **1945**, *17*, 27.
(34) Dash, J. G. *Rev. Mod. Phys.* **1999**. *71*. 1737.
(35) Buschow, K. H. J.; de Boer, F. R. *Physics of Magnetism and Magnetic Materials*: Kluwer Acad. Pub.: New York, 2004.
(36) Sommerfeld, A.; Bethe, H. In *Handbook of Physics*; Geiger, H., Schell, K., Eds.; Springer: Berlin, 1936; Vol. 24, p 595.
(37) Jiang, Q.; Ao, Z. M.; Zheng, W. T. *Chem. Phys. Lett.* **2007**, *439*, 102.
(38) Herr, U.; Jing, J.; Birringer, R.; Gonser, U.; Gleiter, H. *Appl. Phys. Lett.* **1987**, *50*, 472.
(39) Childress, J. R.; Chien, C. L.; Zhou, M. Y.; Sheng, P. *Phys. Rev. B* **1991**, *44*, 11689.
(40) Hou, M.; Azzaoui, M. E.; Pattyn, H.; Verheyden, J.; Koops, G.; Zhang, G. *Phys. Rev. B* **2000**, *62*, 5117.
(41) Sun, C. Q. *Prog. Solid. State Chem.* **2007**, *35*, 1.
(42) Shi, F. G. *J. Mater. Res.* **1994**, *9*, 1307.
(43) Jiang, Q.; Tong, H. Y.; Hsu, D. T.; Okuyama, K.; Shi, F. G. *Thin Solid Films* **1998**, *312*, 357.
(44) Jiang, Q.; Shi, H. X.; Zhao, M. *J. Chem. Phys.* **1999**, *111*, 2176.
(45) Lang, X. Y.; Zheng, W. T.; Jiang, Q. *Phys. Rev. B* **2006**, *73*, 224444.
(46) Regel′, A. R.; Glazov, V. M. *Semiconductors* **1995**, *29*, 405.
(47) Mott, N. F. *Proc. R. Soc. London, Ser. A* **1934**, *146*, 465.
(48) Tiwari, G. P.; Juneja, J. M.; Iijima, Y. *J. Mater. Sci.* **2004**, *39*, 1535.
(49) Buckwald, R. A.; Hirsch, A. A.; Cabib, D.; Callen, E. *Phys. Rev. Lett.* **1975**, *35*, 878.
(50) Jensen, P. J.; Dreyssé, H.; Kiwi, M. *Eur. Phys. J. B* **2005**, *46*, 541.
(51) Yang, C. C.; Jiang, Q. *Acta Mater.* **2005**, *53*, 3305.
(52) Zhang, R. J.; Willis, R. F. *Phys. Rev. Lett.* **2001**, *86*, 2665.
(53) Lang, X. Y.; Jiang, Q. *J. Nanopart. Res.* **2007**, *9*, 595.
(54) Jiang, Q.; Lu, H. M.; Zhao, M. *J. Phys.: Condens. Matter* **2004**, *16*, 521.
(55) Zhong, W. H.; Sun, C. Q.; Li, S.; Bai, H. L.; Jiang, E. Y. *Acta Mater.* **2005**, *53*, 3207.
(56) Pauling, L. *J. Am. Chem. Soc.* **1947**, *69*, 542.
(57) Goldschmidt, V. M. *Ber. Dtsch. Chem. Ges.* **1972**, *60*, 1270.
(58) Billas, I. M. L.; Chatelain, A.; de Heer, W. A. *Science* **1994**, *265*, 1682.
(59) Sun, C. Q.; Li, S.; Li, C. M. *J. Phys. Chem. B* **2005**, *109*, 415.
(60) Nikolaev, V. I.; Shipilin, A. M. *Phys. Solid. State* **2003**, *45*, 1079.
(61) Tang, Z. X.; Sorensen, C. M.; Klabunde, K. J.; Hadjipanayis, G. C. *Phys. Rev. Lett.* **1991**, *67*, 3602.
(62) http://www.webelements.com/.